Stabilization of *Torpedo californica* Acetylcholinesterase by Reversible Inhibitors[†]

Lev Weiner,*[,‡] Valery L. Shnyrov,[||] Leonid Konstantinovskii,[‡] Esther Roth,[§] Yacov Ashani,[§] and Israel Silman[§]

Chemical Research Support and Department of Neurobiology, Weizmann Institute of Science, Rehovot 76100, Israel, and Department of Biochemistry and Molecular Biology, Universidad de Salamanca, Salamanca 37007, Spain

Received June 26, 2008; Revised Manuscript Received September 17, 2008

ABSTRACT: The dimeric form of *Torpedo californica* acetylcholinesterase provides a valuable experimental system for studying transitions between native, partially unfolded, and unfolded states since long-lived partially unfolded states can be generated by chemical modification of a nonconserved buried cysteine residue, Cys 231, by denaturing agents, by oxidative stress, and by thermal inactivation. Elucidation of the 3D structures of complexes of *Torpedo californica* acetylcholinesterase with a repertoire of reversible inhibitors permits their classification into three categories: (a) active-site directed inhibitors, which interact with the catalytic anionic subsite, at the bottom of the active-site gorge, such as edrophonium and tacrine; (b) peripheral anionic site inhibitors, which interact with a site at the entrance to the gorge, such as propidium and *d*-tubocurarine; and (c) elongated gorge-spanning inhibitors, which bridge the two sites, such as BW284c51 and decamethonium. The effects of these three categories of reversible inhibitors on the stability of *Torpedo californica* acetylcholinesterase were investigated using spectroscopic techniques and differential scanning calorimetry. Thermodynamic parameters obtained calorimetrically permitted quantitative comparison of the effects of the inhibitors on the enzyme's thermal stability. Peripheral site inhibitors had a relatively small effect, while gorge-spanning ligands and those binding at the catalytic anionic site, had a much larger stabilizing effect. The strongest effect was, however, observed with the polypeptide toxin, fasciculin II (FasII), even though, in terms of its binding site, it belongs to the category of peripheral site ligands. The stabilizing effect of the ligands binding at the anionic subsite of the active site, like that of the gorge-spanning ligands, may be ascribed to their capacity to stabilize the interaction between the two subdomains of the enzyme. The effect of fasciculin II may be ascribed to the large surface area of interaction (>2000 Å^2) between the two proteins. Stabilization of *Torpedo californica* acetylcholinesterase by both divalent cations and chemical chaperones was earlier shown to be due to a shift in equilibrium between the native state and a partially unfolded state (Millard et al. (2003) *Protein Sci. 12*, 2337–2347). The low molecular weight inhibitors used in the present study may act similarly and can thus be considered as pharmacological chaperones for stabilizing the fully folded native form of the enzyme.

The stability of globular proteins is governed by a balance between the destabilization conferred by conformational entropy and the stabilization conferred primarily by hydrogen bonding and by hydrophobic interactions (*1*). Consequently, the conformational stability of most proteins is quite low, of the order of 5−15 kcal mol^{-1}, and enhancing their stability is of great importance in a biotechnological context (*2*). Such stabilization may often be achieved by enzyme inhibitors or metal ions (for a recent example see ref *3*), as well as by appropriate protein engineering (*2*). It has lately been shown that enzyme inhibitors may also be used to assist protein folding *in situ* (*4*); this has led to the emerging strategy of using reversible enzyme inhibitors as pharmacological chaperones for stabilizing the folded form of a protein generated in the endoplasmic reticulum (*5*−*7*). This approach shows special promise for treatment of patients suffering from the lysosomal storage disease, Gaucher disease (*4, 6*).

The principal role of the serine hydrolase, acetylcholinesterase (AChE[1]), is termination of impulse transmission at cholinergic synapses by hydrolysis of the neurotransmitter, acetylcholine (*8*). In keeping with its biological function, it is a very rapid enzyme that exhibits one of the highest known second-order rate constants for the hydrolysis of its physiological substrate, acetylcholine ($k_{cat}/K_m > 5 \times 10^9$ M^{-1} min^{-1}), approaching a rate at which substrate availability is diffusion-controlled (*8*).

[†] This work was supported in part by Grant Number U54NS058183 from the National Institute of Neurological Disorders and Stroke, by the Defense Threat Reduction Agency (DTRA) of the US Army, and by the Benoziyo Center for Neuroscience. V.S. acknowledges travel support from the Kimmelman Center for the Study of Biomolecular Structure and Assembly.

* To whom correspondence should be addressed. Phone: 972-8-934-3410. Fax: 972-8-934-6017. E-mail: Lev.Weiner@weizmann.ac.il.

[‡] Chemical Research Support, Weizmann Institute of Science.

[§] Department of Neurobiology, Weizmann Institute of Science.

[||] Universidad de Salamanca.

[1] Abbreviations: AChE, acetylcholinesterase; *Tc*, *Torpedo californica*; CAS, catalytic anionic subsite; PAS, peripheral anionic site; **N***, quasi-native; **N**, native; **MG**, molten globule; **U**, unfolded; DSC, differential scanning calorimetry; RS-SR, biradical; RS, monoradical; ATC, acetylthiocholine; DTP, 4,4′-dithiopyridine; ANS, 1-anilino-8-naphthalenesulfonic acid; DTNB, 5,5′-dithiobis(2-nitrobenzoic acid); BSA, bovine serum albumin; EDR, edrophonium; DECA, decamethonium; TAC, tacrine; TC, *d*-tubocurarine; BW, BW284c51; PROP, propidium ethiodide; Gdn·HCl, guanidinium hydrochloride; rhAChE, recombinant human acetylcholinesterase; FasII, fasciculin II.

10.1021/bi801196y CCC: $40.75
Published on Web 12/30/2008

Scheme 1

$$\mathbf{N} \Leftrightarrow \mathbf{N^*} \Rightarrow \mathbf{MG} \Leftrightarrow \mathbf{U}$$

The catalytic subunit of AChE contains ~550 amino acid residues (*9*). Solution of the 3D structure of *Torpedo californica* AChE (*Tc*AChE) revealed that it is composed of two subdomains (residues 4−305 and 306−535) and that its active site is buried at the bottom of a deep and narrow gorge that is positioned at the interface of these subdomains (*10, 11*). Inspection of the 3D structure, taken together with site-directed mutagenesis, reveals that residues encompassing almost the entire sequence of the catalytic subunit are required for its function (*12, 13*).

Subsequent solution of the 3D structures of complexes of *Tc*AChE with a repertoire of reversible inhibitors revealed that they can be classified in three categories: (a) active-site directed inhibitors, which interact with the catalytic anionic subsite (CAS), at the bottom of the gorge; (b) peripheral anionic site (PAS) inhibitors, which interact with a site at the entrance to the gorge; (c) elongated gorge-spanning inhibitors, which bridge these two sites (*14*).

It has been shown that chemical modification and physicochemical perturbation can transform native *Tc*AChE into catalytically inactive partially unfolded species that are long-lived under physiological conditions, permitting their detailed physicochemical characterization (*15*−*17*). Such states can be generated by chemical modification, denaturing agents, oxidative stress, and thermal inactivation (*15*−*18*).

Two principal species were observed, a quasi-native (**N***) state, whose physicochemical characteristics were similar to those of the native (**N**) enzyme (*16*), and a molten globule (**MG**) state, devoid of significant tertiary structure (*15*). The **N*** species transforms spontaneously and irreversibly to the **MG** state, which can, in turn, by more drastic denaturation, be reversibly transformed to an unfolded (**U**) state (*19*). The relationships between these four states can be schematically depicted as shown in Scheme 1 (*20*). *Tc*AChE thus provides a valuable experimental system for studying transitions between native, partially unfolded and unfolded states.

It was earlier shown that chemical chaperones (*21*), as well as divalent cations, can stabilize both the **N** and **N*** states of *Tc*AChE (*20*). As mentioned above, in general, enzyme inhibitors stabilize the structure of their target enzyme (*3*) and may also be used to assist protein folding (*4*). Although some such data exist for AChE (see, for example, refs *11* and *22*), there has been no systematic study of the effects of a repertoire of ligands on the thermal transition and thermodynamic parameters of a purified AChE preparation, although studies of this type have been perfomed on the tetrameric form of human serum butyrylcholinesterase (*23*). In the following, we investigate the effects of the three categories of reversible inhibitors mentioned above on the stability of *Tc*AChE to thermal and chemical denaturation, as well as to inactivation by thiol reagents, using a repertoire of spectroscopic techniques as well as differential scanning calorimetry (DSC).

MATERIALS AND METHODS

Materials. Biradical (RS-SR) and monoradical (RS) were synthesized as described (*24*). Allicin and ^{3}H-allicin were gifts, respectively, from Drs. Aharon Rabinkov and Talia Miron (Weizmann Institute of Science). Acetylthiocholine iodide (ATC), 4,4′-dithiopyridine (DTP), 1-anilino-8-naphthalenesulfonic acid (ANS, magnesium salt), 5,5′-dithiobis(2-nitrobenzoic acid) (DTNB), and bovine serum albumin (BSA) were purchased from Sigma (St. Louis, MO), as were the reversible AChE inhibitors, edrophonium (EDR), decamethonium bromide (DECA), tacrine hydrochloride (TAC), *d*-tubocurarine chloride (TC), and BW284c51 (BW), as well as the irreversible organophosphate inhibitor, paraoxon. Propidium ethiodide (PROP) was obtained from Calbiochem (San Diego, CA). Guanidinium hydrochloride (Gdn·HCl) was from Schwartz/Mann Biotech (Cleveland, Ohio).

*Tc*AChE was the dimeric (G_2) glycosylphosphatidylinositol-anchored form purified from electric organ tissue of *T. californica* by affinity chromatography subsequent to solubilization with phosphatidylinositol-specific phospholipase C (*25*). Concentrations of stock solutions were determined by titration with paraoxon (*O*,*O*-diethyl-*O*-[4-nitrophenyl]phosphate), according to the procedure of Ralston et al. (*26*). Recombinant human AChE (rhAChE), expressed in *Drosophila* S2 cells, and purified as described (*27*), was a gift from by Dr. Terry Rosenberry (Mayo Clinic, Jacksonville, FL). Fasciculin II (FasII), from *Dendroaspis angusticeps*, was obtained from Alamone Laboratories (Jerusalem, Israel) as a lyophilized preparation. The lyophilized toxin (70 μg) was dissolved in deionized water (1 mL) containing 0.025% BSA, and stored at −20 °C. Freshly prepared working solutions were prepared by dilution of the stock solution into deionized water containing 0.025% BSA, and were calibrated against rhAChE solutions whose concentration had been determined by titration with paraoxon, assuming 1:1 stoichiometry for inhibition by FasII (*28*).

Determination of Inhibition Constants. The inhibition constant, K_I, for inhibition of *Tc*AChE by FasII was determined by two methods, both carried out in 0.025% BSA/0.01% NaN_3/50 mM phosphate, pH 8.0, at 25 °C.

Method A: Solutions of 0.02−0.035 nM *Tc*AChE were preincubated for 15 min, in a 1 mL cuvette, with increasing concentrations of FasII. Residual activity was then measured in the presence of 0.02−0.07 mM ATC by a standard protocol (*29*). The slopes and *y*-intercepts of the Lineweaver−Burk plots versus FasII were used to determine K_I values.

Method B: Preincubation of *Tc*AChE with FasII was as in Method A, but residual AChE activity was measured at a single ATC concentration (0.5 mM). K_I was calculated from the following equation:

$$K_I = [E_{eq}][I_0 - EI_{eq}]/[EI_{eq}] \quad (1)$$

where $[E_{eq}]$, $[EI_{eq}]$, and $[I_0 - EI_{eq}]$ are, respectively, the equilibrium concentrations of the free enzyme, the FasII/*Tc*AChE complex, and FasII, assuming 1:1 binding stoichiometry.

Since Tris buffer was used for the unfolding experiments with Gdn·HCl, the dissociation constants for tacrine, BW284c51, and Gdn·HCl were determined in 0.025% BSA/0.01% sodium azide/0.6 M NaCl/10 mM Tris, pH 8.0, at 25 °C. Briefly, increasing fixed concentrations of the inhibitors were used to construct the 1/*V* versus 1/*S* Lineweaver−Burk plots, and K_I was then calculated from the replots of the slope and from the *y*-intercepts of the Lineweaver−Burk plots versus the ligand concentrations (*30*).

Table 1: Dissociation Constants of the Reversible Complexes of *Tc*AChE with BW, TAC, and Gdn·HCl[a]

	K_I[b] (nM)		αK_I[b] (nM)		
ligand	0.1 M NaCl	0.6 M NaCl	0.1 M NaCl	0.6 M NaCl	binding stoichiometry[c]
BW	4.6	44.7	3.5	34.1	1.05
TAC	6.4	21.1	7.4	18.6	0.98
Gdn·HCl	18.1 mM	35.1 mM	NA[d]	NA[d]	1.03

[a] 0.01% azide/0.025% BSA/10 mM Tris chloride, pH 8.0, 25 °C. [b] K_I and αK_I are the dissociation constants of the [ligand][*Tc*AChE] and [ligand][*Tc*AChE][substrate] complexes, respectively (*30*). [c] [Ligand]/[*Tc*AChE] molar ratio. [d] Not applicable; competitive inhibitor.

ESR Spectroscopy. ESR spectra were measured in 70 μL flat quartz cells at room temperature, using a Bruker ER200D-SRC spectrometer. A stock solution of 5 mM biradical in ethanol was diluted to 20 μM in 10 mM Hepes, pH 7.2, and added to 6 μM *Tc*AChE in the same buffer. The instrumental parameters were as follows: microwave frequency, 9.7 GHz; microwave power, 10 mW; modulation amplitude, 1 G; receiver gain, 6.3×10^4.

NMR Spectroscopy. Spectra were recorded on a Bruker Avance-500 spectrometer, equipped with a dedicated TXI-microprobe; 2.5 mm NMR tubes were used, permitting the use of sample volumes as small as 120 μL.

Solutions of samples were prepared in 99.8% deuterium oxide/10 mM phosphate; pD = 7.3. The ^{1}H- and ^{13}C NMR signals of tacrine were assigned on the basis of its DEPT, g-COSY, g-HSQC, and g-HMBC spectra.

Differential Scanning Calorimetry. The calorimetric experiments were performed on a MicroCal MC-2D differential scanning microcalorimeter (MicroCal Inc., Northampton, MA) with cell volumes of 1.22 mL, interfaced with a IBM-compatible personal computer, as described previously (*20*). Scan rates in the range of 0.5−1.5 K/min were employed. Before measurement, sample and reference solutions were degassed in an evacuated chamber for 5 min at room temperature and carefully loaded into the cells to avoid bubble formation. Exhaustive cleaning of the cells was undertaken before each experiment. An overpressure of 2 atm of dry nitrogen was maintained over the sample solutions throughout the scans to prevent any degassing during heating. A background scan collected with a buffer in both cells was subtracted from each scan. Reversibility of the thermal transition was checked by performing the scan a second time, immediately after the sample had cooled subsequent to the first scan. The experimental calorimetric traces were corrected for the effect of instrument response time (*31*). The excess heat capacity functions were plotted after normalization (M = 65,000 g/mol of monomer) and chemical baseline subtraction using the Windows-based software package (Origin) supplied by MicroCal. As in our earlier studies on *Tc*AChE (*18, 20*), only one model was considered in analyzing the data. This is an irreversible, kinetically controlled two-state model in which only the native state and the final (irreversibly denatured) state are significantly populated, and conversion from the native to the denatured state is determined by a strongly temperature-dependent, first-order rate constant, k; this rate constant is given by the Arrhenius equation:

$$k = \exp\{E_A(1/T^* - 1/T)/R\} \quad (2)$$

where R is the gas constant, E_A is the activation energy of the denaturation process, and T^* is the temperature at which $k = 1$ min^{-1}. The rate constant can also be determined by the equation derived on the basis of the activated-complex theory (*32*):

$$k = (k_B T/h) \exp(\Delta S^{\#}/R) \exp(-\Delta H^{\#}/RT) \quad (3)$$

where k_B is the Boltzmann constant, h is the Planck constant, and $\Delta S^{\#}$ and $\Delta H^{\#}$ are, respectively, the entropy and enthalpy of activation.

The Arrhenius equation parameters, E_A and T^*, were obtained by nonlinear least-squares fitting of the equation for the excess heat capacity, C_p^{ex} (*33*):

$$C_p^{ex} = \frac{1}{\upsilon}\Delta H \exp\left\{\frac{E_A}{R}\left(\frac{1}{T^*} - \frac{1}{T}\right)\right\} \times \exp\left\{-\frac{1}{\upsilon}\int_{T_o}^{T} \exp\left[\frac{E_A}{R}\left(\frac{1}{T^*} - \frac{1}{T}\right)\right] dT\right\} \quad (4)$$

where $\nu = dT/dt$ (K/min) is the scan rate, and ΔH is the enthalpy difference between the denatured and native states.

Thermal Inactivation of TcAChE. *Tc*AChE (3.5 nM) in 0.025% BSA/0.01% sodium azide/50 mM phosphate, pH 8.0, was incubated for 10 min at 25 °C, in the absence or presence of FasII, and then transferred to 40 °C. To determine residual enzyme activity, 10 μL aliquots were diluted, at appropriate times, into 1 mL of 0.025% BSA/0.01% sodium azide/50 mM phosphate, pH 8.0, and then incubated for 6 min, so as to allow complete reequilibration of the FasII/*Tc*AChE complex, prior to the addition of the Ellman assay mixture, with ATC at a final concentration of 0.5 mM. The thermal protection conferred by TAC was determined by the same protocol, except that residual enzyme activity was assayed immediately following dilution into the assay buffer.

Denaturation by Gdn·HCl. The fluorescence of 0.24 mL of 100 μM ANS in 0.75 M Gdn·HCl/10 mM Tris, pH 8.0, was monitored for 0.75−1.5 min to determine baseline intensity. Denaturation was initiated by rapid mixing of 60 μL of a solution of *Tc*AChE, in the presence or absence of an inhibitor, with the ANS/Gdn·HCl solution, to yield a final concentration of 1.5 μM *Tc*AChE in 0.6 M Gdn·HCl. The increase in ANS fluorescence was then monitored for 3 min.

RESULTS

Reversible Inhibition. BW (*34*) and TAC (*35*) are both well-known reversible inhibitors of AChE. Nevertheless, for the present study we considered it necessary to accurately assess their inhibitory capacity for *Tc*AChE under the experimental conditions employed. Table 1 shows the values of K_I and of αK_I (the dissociation constant of the ternary enzyme−inhibitor−substrate complex) obtained for the two inhibitors and for Gdn·HCl.

Although inhibition of AChE by FasII has been studied in detail for various wild-type and mutant mammalian and

fish AChEs (*28, 36*−*39*), no full kinetic characterization has been performed for *Tc*AChE.

As described under Materials and Methods, two methods were used to determine the K_I of FasII for *Tc*AChE. Using Method A, it was shown that FasII did not affect K_m, but reduced V_{max}. This apparent noncompetitive mode of inhibition yielded a K_I value of 0.15 ± 0.05 nM. Similar values, 0.14 and 0.36 nM, were reported for *Torpedo marmorata* AChE and for *Electrophorus electricus* AChE by Cousin et al. (*40*) and by Golicnik and Stojan (*39*), respectively. Mammalian AChEs are 14- to 25-fold more sensitive to FasII than *Tc*AChE (*28, 36*). Cousin et al. (*40*) reported only an αK_I value (for dissociation of the ternary [E][FasII][ATC] complex), suggesting that the same slopes were obtained for the Lineweaver−Burk plots at different FasII concentrations. Such parallel lines would suggest uncompetitive inhibition, i.e., that the inhibitor would bind only to the ES complex, which seems most unlikely. Unlike with *Electrophorus* AChE (*39*) and mammalian AChEs (*28, 36*), the rate of approach to steady state with *Tc*AChE in the presence of FasII was rapid and, under the experimental conditions employed, precluded accurate separation of the individual rate constants for the association and dissociation of FasII (not shown).

Using Method B, a K_I value of 0.16 ± 0.01 nM (SE, n = 13) was obtained. The number of binding sites for FasII was calculated from the slope of the straight line obtained by plotting $\log[(V_0/V_{FasII}) - 1]$ vs log[FasII]. A value of 1.01 ± 0.09 (SE, n = 13) was obtained. The close agreement between the K_I values obtained by the two methods is consistent with apparently noncompetitive inhibition in which ATC and FasII both bind reversibly and randomly at separate sites, and the dissociation constants of the [E][FasII] and [E][FasII][ATC] complexes are indistinguishable.

Chemical Modification. We earlier showed that chemical modification by thiol reagents, which can modify the buried and nonconserved Cys231 residue in *Tc*AChE, deactivates the enzyme (*15, 41*). Concomitant with deactivation there is a transition to one of two partially unfolded states, either **N*** or **MG**. Mercurials and allicin produce the **N*** state, which subsequently decays to an **MG** state (*16, 20*), whereas various alkylating reagents, such as *N*-ethylmaleimide, produce an **MG** state directly (*15, 16*).

Modification of *Tc*AChE by the disulfide reagent, DTP, directly produces the **N**→**MG** transition (*15*). Figure 1 shows the effect of two reversible inhibitors (BW and DECA) on the deactivation of *Tc*AChE by DTP. Both inhibitors significantly slowed the inactivation of the enzyme and thus blocked the transition.

As already mentioned, modification by the reactive thiosulfinate, allicin, initially results in the **N**→**N*** transition, with concomitant deactivation (*20*). Figure 2 shows that in this case, too, deactivation can be strongly retarded by the reversible inhibitor, BW.

The question arose whether retardation of deactivation was due to the prevention of chemical modification or to the arrest of a conformational transition of the chemically modified enzyme from an active to an inactive state. This issue was addressed by making use of the nitroxyl-containing disulfide reagent, biradical (*24*) (Scheme 2). This reagent can be used to titrate sulfhydryl groups using ESR and also to spin-label cysteine residues in proteins (*42, 43*).

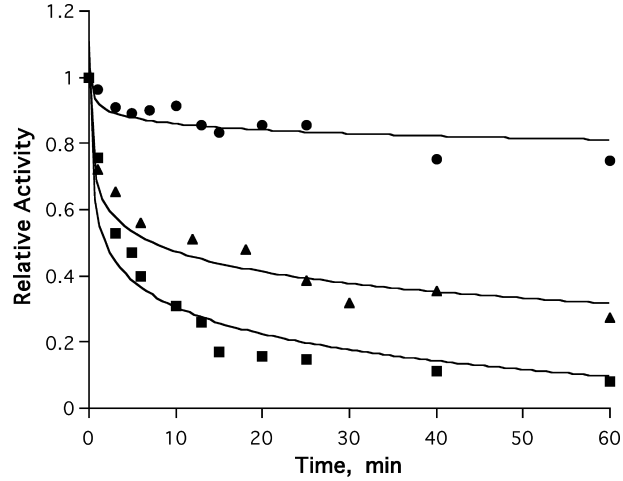

FIGURE 1: Protection by ligands against DTP-induced inactivation of *Tc*AChE. *Tc*AChE (2 μM) was inhibited by 2 mM DTP in 0.01% NaN_3/0.1 M NaCl/10 mM sodium phosphate, pH 7.0, at 23 °C. ■-■-■, *Tc*AChE + DTP alone; ●-●-●, *Tc*AChE + 20 μM BW+DTP; ▲-▲-▲, *Tc*AChE + 20 μM DECA+DTP.

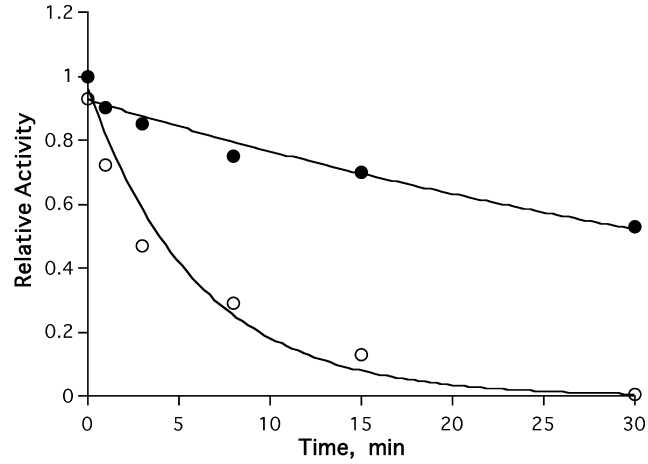

FIGURE 2: Effect of BW on the rate of inactivation of *Tc*AChE by allicin.○-○-○, 2 mM allicin; ●-●-●, 2 mM allicin + 20 μM BW. Experimental conditions are as described in Figure 1.

Indeed, we earlier showed that the biradical, like DTP, can covalently label Cys231 in *Tc*AChE, with concomitant deactivation and transition to a **MG** state (*15*). The stable, nonactive free thiol, R•SH (*42*), released during the reaction, can be detected due to the appearance of the narrow and strong monoradical ESR signal.

Figure 3 shows the rate of appearance of the monoradical signal upon reaction of the biradical with *Tc*AChE in both the absence and presence of BW. It can be seen that there is no detectable difference in the rate of modification in the two samples. Thus, clearly, the BW has no effect on the rate of chemical modification and must, therefore, be acting by retarding the rate of transition of the enzyme from an active to an inactive conformation, presumably the **MG** state (*15, 16*).

Figure 4 makes use of ^{3}H-allicin to show that inactivation of *Tc*AChE by allicin is accompanied by stoichiometric covalent binding of allicin to the enzyme, most likely by thiol-disulfide exchange with Cys231, as was demonstrated

Scheme 2

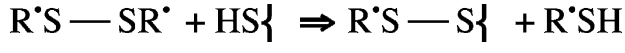

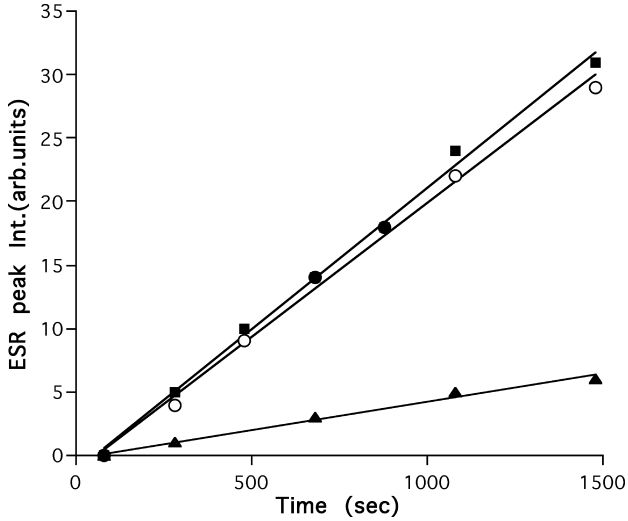

FIGURE 3: Rate of modification of *Tc*AChE by the spin-labeled disulfide, biradical, in the presence and absence of BW. The traces display the rates of appearance of monoradical, monitored by EPR, using 20 μM biradical and 5 μM *Tc*AChE, in 10 mM phosphate, pH 7.4, in the presence (■-■-■) and absence (○-○-○) of 16 μM BW. The lower trace (▲-▲-▲) is a control showing the rate of spontaneous appearance of the monoradical in the absence of enzyme.

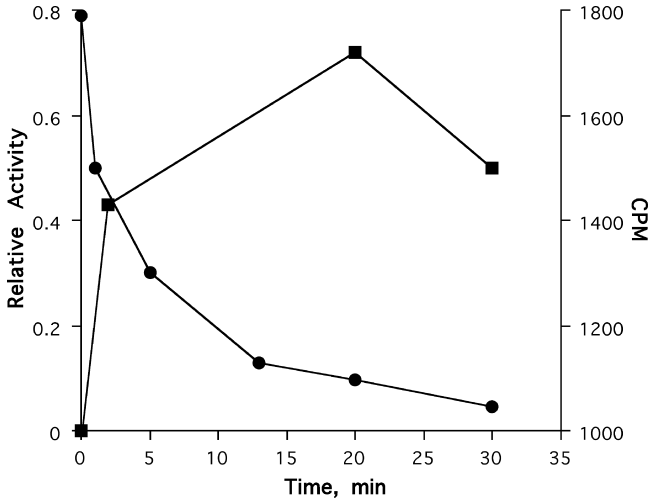

FIGURE 4: Kinetics of inactivation of *Tc*AChE by allicin and of covalent binding of radioactive allicin to the enzyme. ●-●-●, inactivation of 0.17 mM *Tc*AChE in 0.01% NaN_3/0.1 M NaCl/10 mM phosphate, pH 7.0, at 23 °C by 4 mM allicin; ■-■-■, incorporation into *Tc*AChE of ^{3}H-allicin. *Tc*AChE (0.17 mM) in 0.1 M NaCl/10 mM phosphate, pH 7.0, was incubated with 4 mM ^{3}H-allicin at 23 °C. Aliquots were removed at the appropriate time and the levels of labeled ligand bound determined as described under Materials and Methods.

for both the biradical and DTP (*15, 16*). ^{3}H-allicin (*44*) was also used to demonstrate that BW does not protect against chemical modification but only against the conformational transition to an inactive form (not shown).

Gdn·HCl Denaturation. We earlier showed that exposure of *Tc*AChE to Gdn·HCl produced a **N→MG** transition (*15, 16*). In the **MG** state, *Tc*AChE displays exposed hydrophobic surfaces whose appearance can be monitored by use of the amphipathic probe, ANS (*15, 16*). Figure 5A shows the time course of increase in ANS fluorescence following the addition of Gdn·HCl (final concentration 0.6 M) to a solution of *Tc*AChE in the presence and absence of TAC. For *Tc*AChE alone, a sharp ~5-fold increase in ANS fluorescence

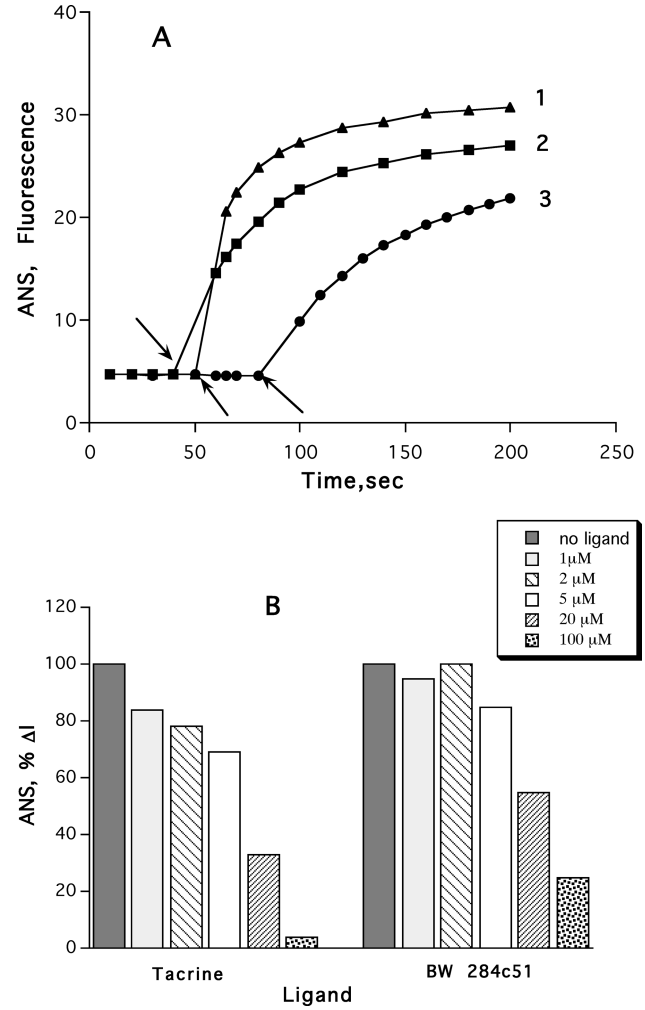

FIGURE 5: Protection by AChE inhibitors against unfolding of *Tc*AChE by 0.6 M Gdn·HCl. Panel A: Rate of increase in ANS fluorescence of *Tc*AChE produced by addition of the 0.6 M Gdn·HCl to *Tc*AChE. An ANS/Gdn·HCl solution was added to a solution of *Tc*AChE, in the presence or absence of TAC, as described under Materials and Methods. 1. Control, in the absence of ligand. 2. Final TAC concentration, 5 μM. 3. Final TAC concentration, 20 μM. Panel B: Bargraph representation of the increase in ANS fluorescence produced at 20 s after the addition of 0.6 M Gdn·HCl to the *Tc*AChE solution at the appropriate concentrations of TAC and BW. Experimental conditions are as in (A). 100% denotes the average increase in fluorescence intensity (ΔI) obtained in the absence of ligand ($n = 3$).

was observed, followed by a second slower phase. If the same experiment was performed with *Tc*AChE that had been preincubated with TAC, both the initial jump in ANS fluorescence and the rates of the first and second phases were decreased in a concentration-dependent manner. BW produced very similar data (not shown). Figure 5B shows the relative decreases in ANS fluorescence produced by increasing concentrations of TAC and BW, as compared to the control value, at 20 s after addition of Gdn·HCl. Addition of either TAC or BW to a solution of *Tc*AChE in 0.6 M Gdn·HCl, in the presence of ANS, did not reduce the intensity of ANS fluorescence, showing that neither of these ligands could displace the bound ANS from the partially unfolded enzyme.

It should be noted that, despite the high calculated occupancy of *Tc*AChE by 5 and 20 μM TAC and BW (>99.5% based on the K_I values shown in Table 1), if an

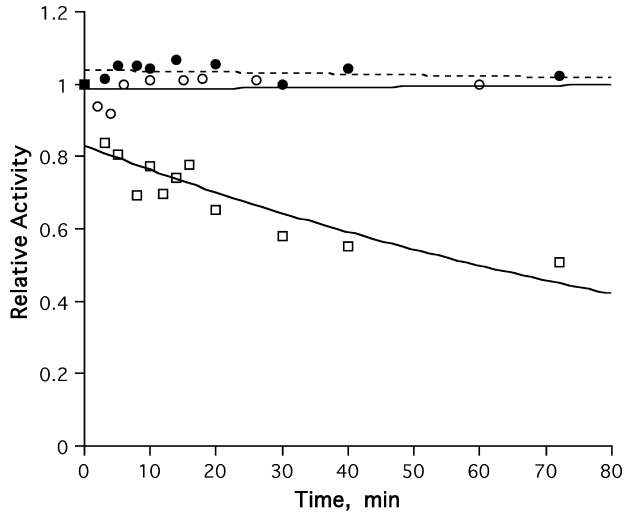

FIGURE 6: Protection by TAC against inactivation of *Tc*AChE by Gdn·HCl as monitored by the decrease in enzymic activity. *Tc*AChE (2 μM) in 0.01% NaN_3/0.1 M NaCl/10 mM phosphate, pH 7.0, containing 0.6 M Gdn·HCl was incubated at 23 °C in the presence and absence of 50 μM TAC. ○-○-○, control (*Tc*AChE alone); □-□-□, 0.6 M Gdn·HCl; ●-●-●, 0.6 M Gdn·HCl + 50 μM TAC.

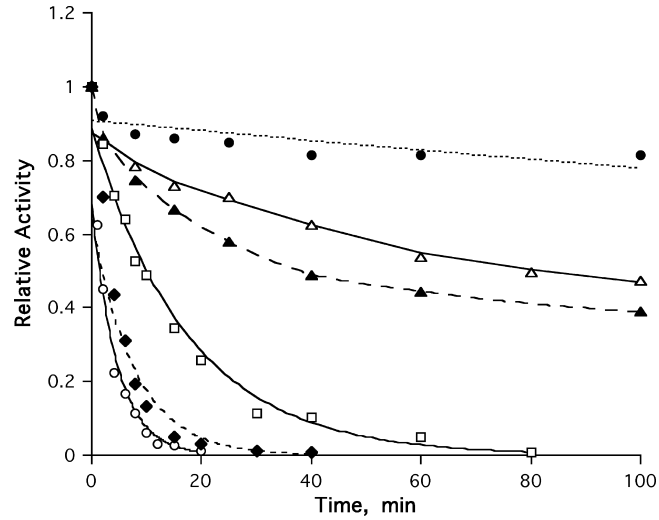

FIGURE 7: Retardation of thermal denaturation of *Tc*AChE by reversible inhibitors. *Tc*AChE (3 μM) in 0.01% NaN_3/0.1 M NaCl/10 mM phosphate, pH 7.0, was incubated at 39 °C in the presence or absence of ligands, and aliquots were removed for assay at the appropriate times. ○-○-○, control (without ligand); ◆-◆-◆, 50 μM TC; □-□-□, 50 μM GAL; ▲-▲-▲, 20 μM EDR; △-△-△, 20 μM DECA; ●-●-●, 20 μM BW.

even larger excess of inhibitor was employed (100 μM, viz. a >60-fold molar ratio over *Tc*AChE), a further decrease in ANS fluorescence intensity was observed (Figure 5B). Notably, the ratio, [Gdn·HCl]/K_{Gdn} = 17, was substantially lower than [ligand]/K_{ligand} (>2800 at 100 μM); this suggests that high concentrations of both ligands are required to kinetically compete out the association of Gdn·HCl with *Tc*AChE in the rate-limiting step of enzyme inactivation due to unfolding and thereby to confer complete protection by their presence within the active-site region. We cannot rule out the possibility that saturation of the PAS, or of another ligand-binding site influencing stability, might contribute to the thermal stabilization, an effect that would be recognized experimentally only at high ligand concentrations. Overall, the data presented indicate that full occupancy of the CAS by either of the two reversible ligands can significantly protect against unfolding by Gdn·HCl.

Protection against Gdn·HCl denaturation by TAC was also assessed by monitoring the rate of disappearance of enzymic activity. Figure 6 shows that the rate of inactivation at 50 μM TAC, at which concentration it can be calculated that occupancy of the anionic subsite of the active site is well over 99%, protection against loss of enzymic activity is virtually complete.

Thermal Denaturation. *Tc*AChE has been shown to undergo irreversible thermal denaturation that can be described by a two-state model (*20, 23*). Figures 7−9 show that thermal denaturation, too, can be retarded by reversible inhibitors of AChE. However, an interesting pattern emerges. Although all of these inhibitors were utilized at saturating concentrations based on their inhibition constants, the active-site directed inhibitors, EDR and TAC, and the two gorge-spanning inhibitors, DECA and BW, retarded thermal deactivation strongly, whereas the two peripheral anionic site inhibitors, TC and gallamine, had a relatively weak effect (Figure 7). Figure 8A shows the protective effect exerted by DECA at three different temperatures. Similar experiments were also performed for the other inhibitors and permitted the construction of Arrhenius plots (Figure 8B) from which values of E_A could be extracted. The values were 85 ± 10 kcal/mol and 167 ± 15 kcal/mol, respectively.

As mentioned above, FasII is a very powerful inhibitor of vertebrate AChEs, with K_i values in the lower pM range (*28, 36*). Figure 9 shows that even at 40 °C FasII protects *Tc*AChE against thermal denaturation. Thus, if the concentration of ligand was both much greater than that of the enzyme and of its K_i value, resulting in >99% saturation of the binding site, essentially complete protection was obtained. Under the experimental conditions employed, with *Tc*AChE = 3.5 nM, this could be achieved using 1.5 μM TAC (Figure 9A) or 50 nM FasII (Figure 9B).

Figure 10 shows protection against inactivation by the gorge-spanning ligand, DECA (*45*), the divalent cation, Mn^{2+}, and the two together. Divalent metal ions are known to stabilize *Tc*AChE very strongly (*20*) and do so by binding at a site distinct from both the active site and the PAS (Nicolas, A., personal communication). Thus, it is not unexpected that the two ligands act synergistically.

Calorimetric Measurements. The thermal denaturation of intact and inhibitor-modified *Tc*AChE at pH 7.0 gives rise to well-defined DSC transitions (Figure 11), whose apparent T_m (temperature at the maximum of the heat capacity profile) depends on the scan rate (data not shown). In all cases, thermal denaturation is calorimetrically irreversible, as shown previously (*18*), since no thermal effect was observed if the scan was repeated on the same sample. The effect of the scan rate on the calorimetric profiles (T_m is shifted toward higher temperatures as scanning rate increases) clearly indicates that they correspond to kinetically controlled processes; it is thus evident that equilibrium thermodynamics cannot be applied to their analysis (*46*). Analysis was, therefore, accomplished on the basis of a simple two-state irreversible model (see Materials and Methods). The excess heat capacity functions obtained for *Tc*AChE were analyzed by fitting the data to the two-state irreversible model (eq 4), either individually or globally, using the scan rate as an

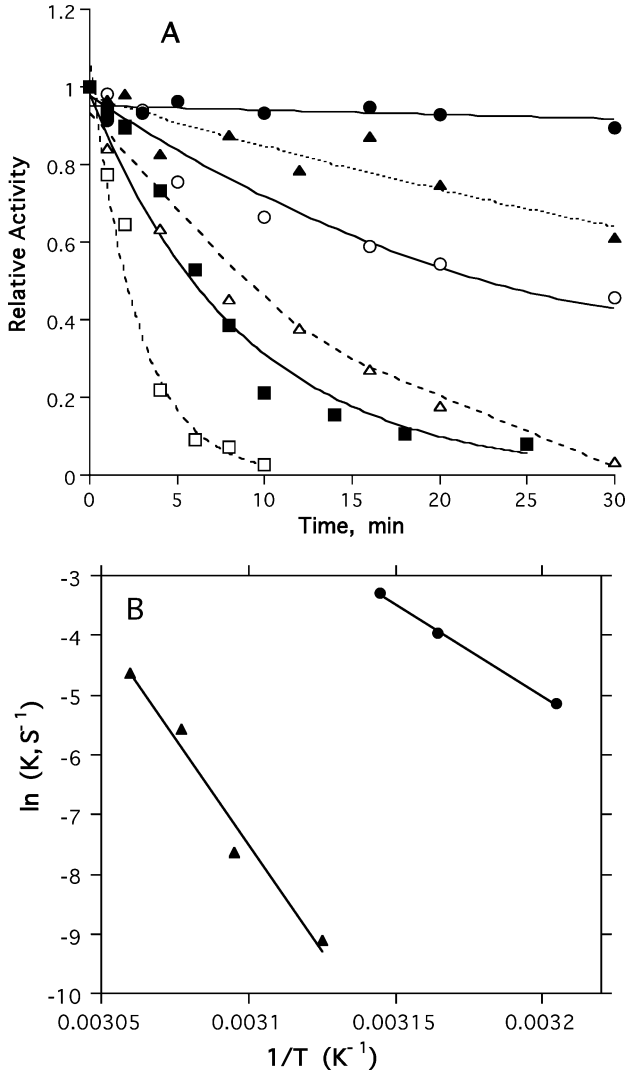

FIGURE 8: Temperature-dependence of thermal denaturation of *Tc*AChE in the absence and presence of DECA. (A) *Tc*AChE (2.5 μM) in 0.01% NaN_3/0.1 M NaCl/10 mM phosphate, pH 7.0, was incubated in the presence and absence of 20 μM DECA. ○-○-○, 39 °C, control; ●-●-●, 39 °C + DECA; △-△-△, 41 °C, control; ▲-▲-▲, 41 °C + DECA; □-□-□, 45 °C, control; ■-■-■, 45 °C + DECA. (B) Arrhenius plots derived from the data shown in (A) obtained in the absence (●-●-●) and presence (▲-▲-▲) of DECA.

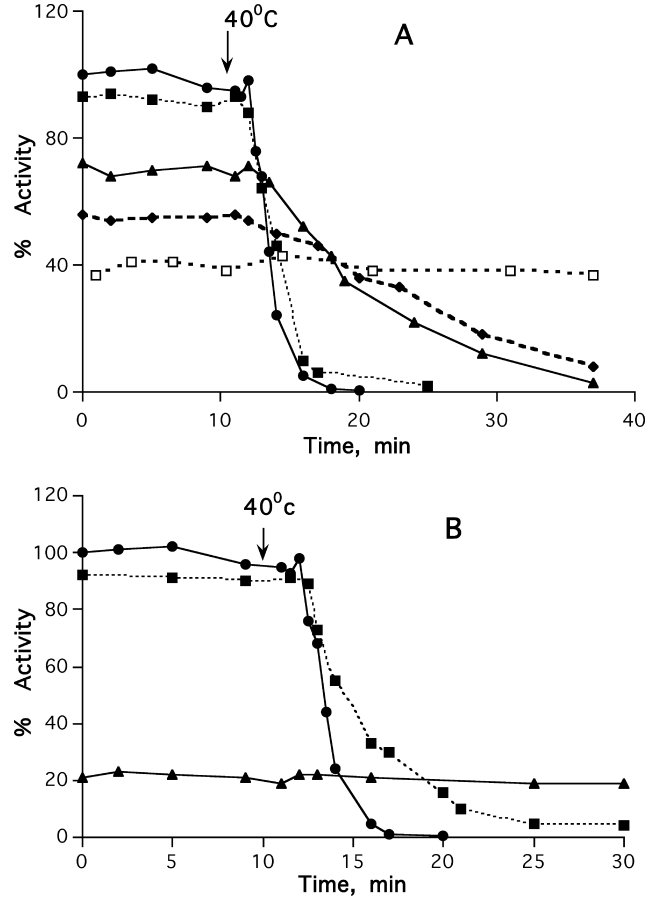

FIGURE 9: Protection of *Tc*AChE against thermal denaturation by FasII and TAC. *Tc*AChE (3.5 nM) was preincubated in 0.025% NaN_3/0.025% BSA/50 mM sodium phosphate, pH 8.0, at 25 °C for 10 min with the appropriate concentrations of TAC or FasII, and then transferred to 40 °C (see arrows). Residual activity was determined at 25 °C following 100-fold dilution into 0.01% NaN_3/0.01% BSA/sodium phosphate, pH 8.0, and 6 min preincubation prior to the addition of the Ellman's reagent reaction mixture, with a final ATC concentration of 0.5 mM. These experimental conditions assured complete reequilibration of the FasII/*Tc*AChE complex. (A) Protection by TAC. ●-●-●, no ligand; ■-■-■, 50 nM TAC; ▲-▲-▲, 330 nM TAC; ◆-◆-◆, 0.5 μM TAC; □-□-□, 1.5 μM tacrine. (B) Protection by FasII. ●-●-●, no ligand; ■-■-■, 7.5 nM FasII; ▲-▲-▲, 50 nM FasII.

additional variable. The lines through the data points in Figure 11 were generated using the results of individual fits. It can be seen that the calculated and experimental curves are in good agreement. Furthermore, no dependence of the shape of DSC transitions on the protein concentration was found in the concentration range of 0.35−1.9 mg/mL.

In the present study, the activated-complex theory (*32*), which describes irreversible denaturation of proteins in terms of thermodynamic parameters, was used to examine how various reversible inhibitors affect thermal denaturation of *Tc*AChE. In accordance with the above-mentioned theory, the rate constant of denaturation, k, can be expressed as shown in eq 3. The value of k can be obtained experimentally from the calorimetric measurements by making use of eq 4 to obtain the Arrhenius parameters and then inserting them into eq 2. Equation 3 can then be used to obtain the values of thermodynamic parameters of activation, $\Delta H^{\#}$ and $\Delta S^{\#}$. The parameters thus obtained are presented in Table 2. Since the values of the parameter, E_A, in eq. 2 are closely related to those of $\Delta H^{\#}$, with the only difference being the value of RT (~0.6 kcal/mol), they are not shown.

FasII has a very pronounced effect on the thermal transition of *Tc*AChE, raising the T_m by more than 16 °C (Figure 11). A control experiment using FasII alone did not reveal any DSC peak for the toxin in the range of 10−100 °C. Thus, the thermal peak observed for the complex can clearly be ascribed to the enzyme.

NMR Spectroscopy. NMR spectroscopy is an effective method for studying the interaction of small ligands with biopolymers (*47*). The method has been applied in only a few cases to the study of AChE−ligand interactions (*48, 49*). Figure 12 displays a portion of the aromatic regions of the NMR spectra of tacrine alone and in the presence of *Tc*AChE. It is clearly seen that binding to the enzyme produces upfield chemical shifts and broadening of all the major peaks. In the presence of an excess of the gorge-spanning ligand, DECA, this effect was practically eliminated (spectrum not shown).

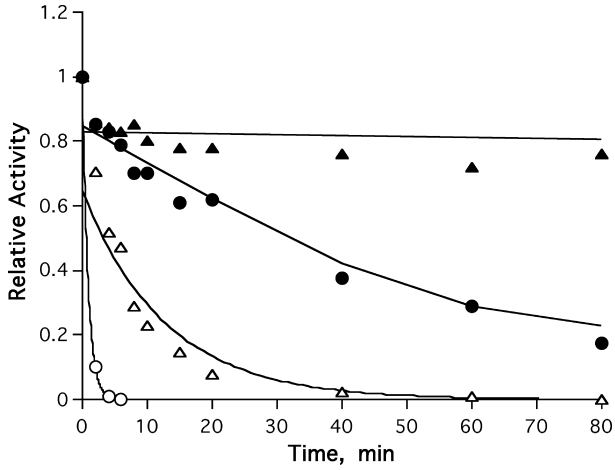

FIGURE 10: Synergistic protection by DECA and Mn^{2+} against thermal inactivation of *Tc*AChE at 43 °C. *Tc*AChE (2 μM) in 0.01% NaN_3/0.1 M NaCl/10 mM phosphate, pH 7.0, was incubated at 43 °C in the absence and presence of 20 μM DECA, 2 mM Mn^{2+}, or both. ○-○-○, control; △-△-△, DECA; ●-●-●, Mn^{2+}; ▲-▲-▲, DECA+Mn^{2+}.

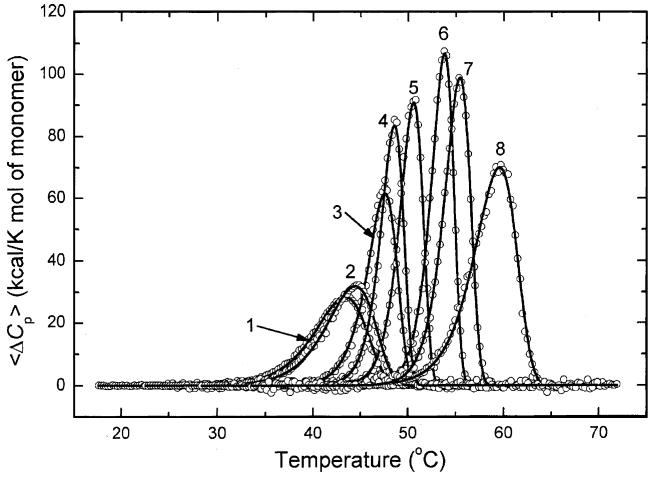

FIGURE 11: Temperature dependence of the excess molar heat capacity of *Tc*AChE and of *Tc*AChE in the presence of various inhibitors. (1) *Tc*AChE alone, and *Tc*AChE in the presence of (2) TC; (3) PRO; (4) DECA; (5) EDR; (6) TAC; (7) BW; (8) FasII. The scan rate was 1 K/min. Solid lines represent the best fits for each calorimetric curve, using eq 4. The *Tc*AChE concentration was ~12 μM. The inhibitors were all at a concentration of 120 μM with the exception of FasII, which was at the same concentration as the enzyme. The buffer employed was 100 mM NaCl/10 mM HEPES, pH 7.0.

DISCUSSION

*Tc*AChE provides a valuable experimental system for studying transitions between native, partially unfolded, and unfolded states because long-lived partially unfolded states can be studied by various methods (*15*−*17, 20*). As already mentioned, such fundamental studies are of special interest in the context of the emerging strategy of using reversible enzyme inhibitors as pharmacological chaperones for stabilizing the folded form of an enzyme generated in the endoplasmic reticulum, an approach that shows special promise for treatment of the lyososomal storage disease, Gaucher disease (*6*). Whereas the **N** state of *Tc*AChE is resistant to proteolysis, the **MG** state is very susceptible (*15*). However, even the **N*** state, although energetically and spectroscopically not very different from the **N** state (*16*), displays enhanced susceptibility to protease treatment (*20*). We earlier presented evidence that divalent cations (Ca^{2+}, Mg^{2+}, and Mn^{2+}) stabilize *Tc*AChE against both thermal denaturation and proteolysis due to their capacity to retard both the **N** → **N*** and the **N*** → **MG** transitions (*20*).

In the present study, we have presented evidence that the conformational transitions initiated by chemical modification of *Tc*AChE, by low concentrations of Gdn·HCl or by elevated temperatures, are affected by the various reversible inhibitors investigated.

Table 2 summarizes the calorimetric data, and certain trends can be distinguished. It can be seen from the table that, with respect to the transition temperature, the two low-molecular-weight PAS inhibitors, TC and PROP, have the smallest effect, and ligands spanning the gorge (DECA and BW) or in the CAS at its base (EDR and TAC), have a stronger influence. Among the low-molecular-weight ligands, BW produces the greatest increase in transition temperature. However, the most dramatic effect is achieved by the polypeptide toxin, FasII, even though, in terms of its binding site, it belongs to the category of PAS ligands. With respect to $\Delta H^{\#}$, low values are observed for the two PAS inhibitors relative to the inhibitors that bind at the CAS or span the CAS and the PAS, in apparent agreement with their low T^* values, but for FasII the value of $\Delta H^{\#}$ is also low, despite its high T^* value. This apparent discrepancy will be discussed below.

For the ligands binding at the PAS, the entropic effects are much smaller than those for the others. PROP has a larger value of $\Delta S^{\#}$ than the other two PAS ligands, possibly due to a contribution of the substantial stacking interaction that it makes with the indole ring of Trp279 (*38*). Although one finger of FasII penetrates the gorge, the interaction of Met33 of the toxin with Trp279 is obviously less substantial. Unfortunately, no crystal structure is yet available for a complex of AChE with TC.

We earlier ascribed the stabilization against denaturation by divalent cations and chemical chaperones to a shift in equilibrium from the **N*** state to the **N** state (see Scheme 1) produced by the bound metal ion (see Scheme 2 in ref *20*). In the case of the metal ions, it was proposed that this is achieved by their tight binding to the **N** state, which increases the value of the Gibbs free energy ($\Delta G^{\#} = \Delta H^{\#} - T\Delta S^{\#}$) between the **N** and **N*** states. It is plausible that the binding of a ligand specific for the enzyme can exert a similar effect.

The principal issue driving the present study is to understand how a quite small ligand can exert such a strong stabilizing effect on a large protein molecule. It is important to clarify that we are not referring to the change in Gibbs free energy between the free enzyme and its complex with the ligand, which can readily be calculated from the dissociation constant (*50*). Values of Gibbs free energy for the ligands in question range from 6.5 kcal/mol for the TC/*Tc*AChE complex to 11.4 kcal/mol for the FASII/*Tc*AChE complex. Rather, we are concerned with the stabilization conferred by a large increase in the energy barrier that needs to be overcome for the conformational transition to occur, viz. $\Delta G^{\#}$ (see Table 2).

The X-ray structure of the TAC/*Tc*AChE complex revealed that the ligand is sandwiched between Trp84 and Phe330 (*45*). The observed chemical shift of the aromatic protons of tacrine (Figure 12) can be ascribed to π-π interactions

Table 2: Kinetic Parameters Estimated for Thermal Denaturation of Native *Tc*AChE and of Its Complexes with Reversible Inhibitors[a]

sample	$\Delta H^{\#}$ (kcal/mol)	$\Delta S^{\#}$ (cal/Kmol)	T^* (°C)	r	K_I
*Tc*AChE	73.5 ±1.6	171.7±0.5	45.9 ± 0.2	0.9984	
*Tc*AChE+TC	79.3 ±1.8	189.0±0.5	47.0 ± 0.2	0.9982	15 μM[b]
*Tc*AChE +PROP	132.7±1.6	354.1±0.5	48.4 ± 0.2	0.9986	2.8 μM[b]
*Tc*AChE +BW	160.8±1.2	430.0±0.6	48.9 ± 0.1	0.9992	0.34 μM[b]
*Tc*AChE+DECA	175.2±1.2	485.5±0.5	51.0 ± 0.2	0.9989	0.15 μM[b]
*Tc*AChE +EDR	176.4±1.4	485.7±0.6	54.1 ± 0.1	0.9991	6.0 nM[c]
*Tc*AChE +TAC	185.8±1.4	509.1±0.7	55.9 ± 0.1	0.9990	4.0 nM[c]
*Tc*AChE +FasII	101.5±1.9	243.8±0.7	62.4 ± 0.2	0.9986	0.4 nM[c]

[a] The data were obtained by DSC as described under Materials and Methods. The parameters were obtained by global fitting of experimental data obtained at three different scan rates (0.5, 1.0, and 1.5 K/min) to a two-state irreversible model (*33*). The experimentally determined inhibition constants of the ligands employed are also presented. $\Delta H^{\#}$ and $\Delta S^{\#}$ are the enthalpy and entropy of activation, respectively, and were estimated using eq 3. T^* is the temperature at which $K = 1$ min^{-1} and was estimated using eq 2. The correlation coefficient (r), which served as criterion for the accuracy of the fits, was calculated as follows

$$r = \sqrt{1 - \sum_{i=1}^{n}(y_i - y_i^{calc})/\sum_{i=1}^{n}(y_i - y_i^{m})^2}$$

where y_i and y_i^{calc} are, respectively, the experimental and calculated values of C_p^{ex}; y_i^m is the mean of the experimental values of C_p^{ex}, and n is the number of points. [b] Ref *53*. [c] Present study.

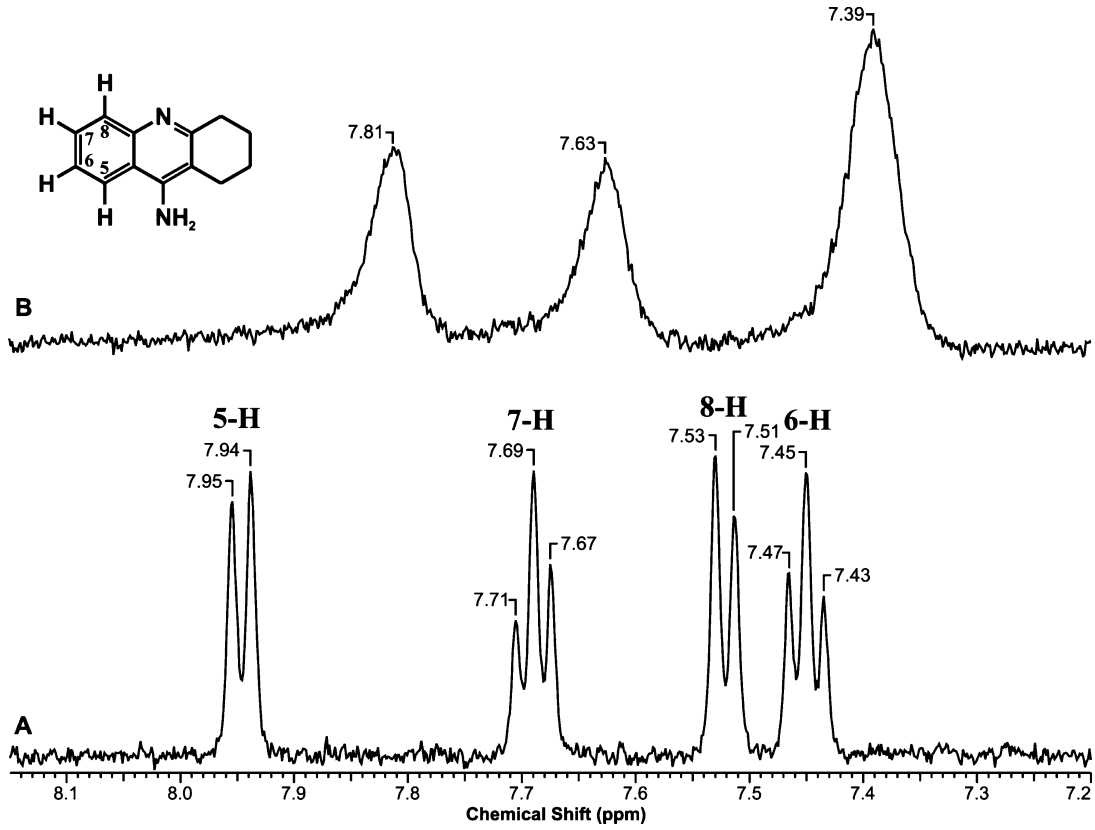

FIGURE 12: Effect on the NMR spectrum of TAC of its association with *Tc*AChE. (A) 0.5 mM TAC in deuterated buffer (see Materials and Methods) at 23 °C; (B) in the presence of 15 μM *Tc*AChE.

with the two aromatic amino acid rings. The broadening of these aromatic proton signals reflects the anticipated loss of mobility due to binding of the small ligand to the protein. It is reasonable to assume that intercalation of the ligand between the two aromatic rings can have a stabilizing effect on the region at the bottom of the active-site gorge. However, inspection of the structure of *Tc*AChE shows that it is composed of two subdomains, corresponding approximately to residues 4−305 and 306−535, which face each other across the active-site gorge (see Figure 13 and ref *11*). Thus, it is plausible that binding of a ligand at this site may freeze the dynamic motions of the entire AChE molecule, with concomitant stabilization, as reflected in our various physicochemical measurements. Global stabilization by other ligands that either bind to the CAS at the bottom of the gorge (e.g., EDR) or span the CAS and the PAS (e.g., BW and DECA), may be similarly explained.

The principal interaction of the PAS ligand, PROP, which binds at the top of the active-site gorge, is with the residues equivalent to Tyr70 and Trp279 in mouse AChE (*40*). These residues are both in the first subdomain, which may explain why it has a smaller stabilizing effect than ligands that span the CAS and PAS or that bridge the two subdomains at the PAS. The same may also be true for TC, but, unfortunately, no 3D structure of a TC/AChE complex is yet available.

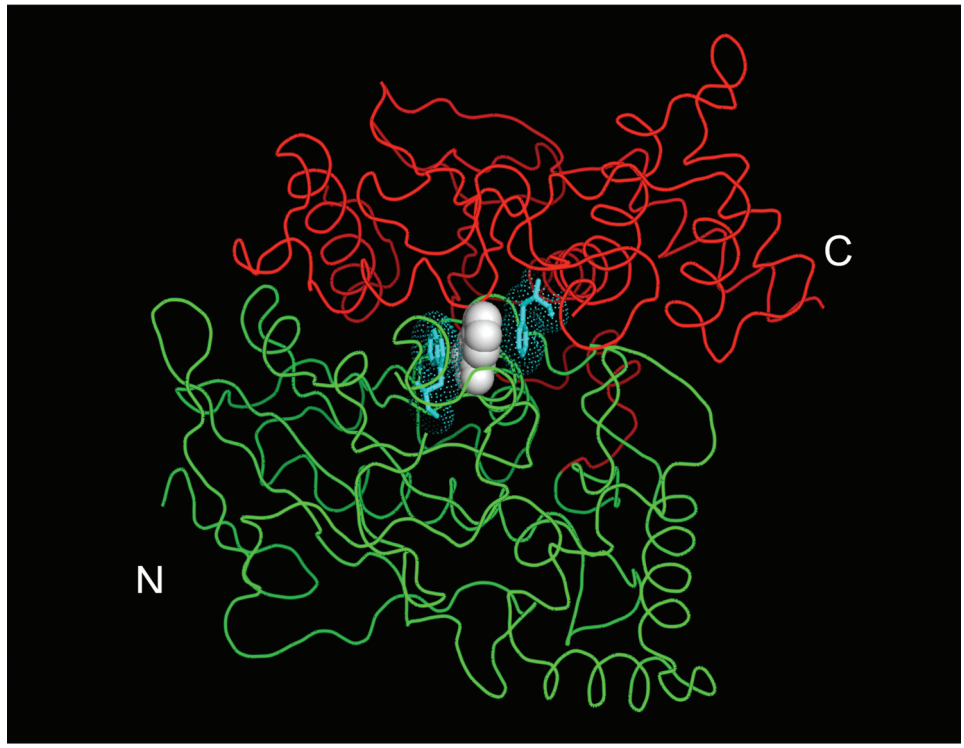

FIGURE 13: Backbone trace of the complex of TAC with *Tc*AChE. The N-terminal subdomain (residues 4−305) is displayed in green, and the C-terminal subdomain (residues 306−535) in red. The bound TAC is shown in a white space-filling representation, sandwiched between Trp84 and Phe330, which are both shown as turquoise sticks with their van der Waals surfaces represented as turqoise dots.

FasII also binds at the PAS, but inspection of its complexes with *Tc*AChE and the mammalian AChEs (*37, 51*) shows that it makes numerous contacts both with residues in the first subdomain (most notably with W279, but also with Tyr70, Gln74, Pro 76, and others) and in the second subdomain (in particular, residues Tyr334 and Gly335) (*37*). These multiple interactions may help to explain why it has both the highest affinity for *Tc*AChE and forms a complex with the highest transition temperature (T^*). However, with the exception of TC, it has the smallest effect on the activation parameters of the transition, viz. $\Delta H^{\#}$ and $\Delta S^{\#}$ (see Table 2). We have no unequivocal explanation for this apparent discrepancy. One possibility is that, due to weakening of the interaction of FasII with the enzyme with increasing temperature, it actually dissociates prior to unfolding of *Tc*AChE. The multiple interactions involved in FasII-*Tc*AChE complexation, involving a total loss of accessible surface area of >2000 Å^2 (*37*), must necessarily result in significant desolvation of the *Tc*AChE molecule. This, in turn, might decrease the cooperativity of the denaturation process (*52*), as is indeed found to be the case (see Figure 11).

It is interesting to note that the values of $\Delta H^{\#}$ and $\Delta S^{\#}$ were found to increase simultaneously, which was due to the compensatory effect (Figure 14). The consistency of the $T\Delta S^{\#}/\Delta H^{\#}$ ratio for denaturation of complexes of *Tc*AChE with different inhibitors suggests that the mechanism of denaturation for all of them (with the possible exception of FasII) is very similar.

We earlier showed that both divalent cations and chemical chaperones can retard the transition of *Tc*AChE to a partially unfolded and enzymatically inactive state (*20*). Here, we have shown that specific inhibitors of the enzyme have a similar effect and that their efficacy can be rationalized in structural terms. Thus, low molecular weight ligands that bridge the two subdomains at the bottom of the active-site gorge seem to be as effective as ligands that span the gorge, whereas ones which bind at the PAS have a much weaker effect.

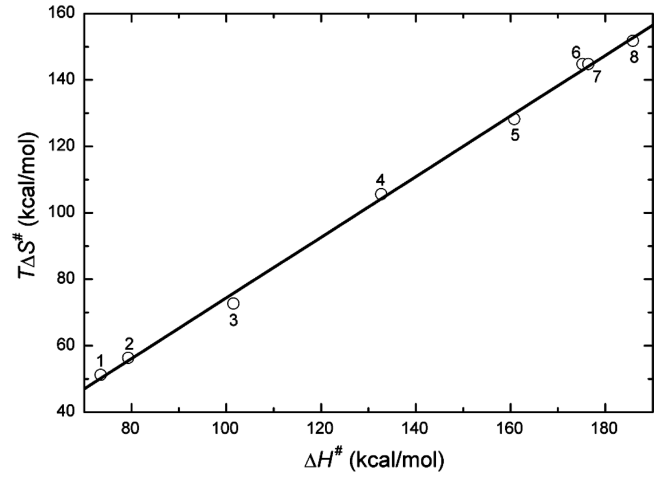

FIGURE 14: Entropy-enthalpy compensation plot for *Tc*AChE and its ligand complexes. $T\Delta S^{\#}$ values are plotted vs $\Delta H^{\#}$ values, both calculated at 298 K. (1) *Tc*AChE alone; (2) + TC; (3) + FasII; (4) + PRO; (5) + BW; (6) + DECA; (7) + EDR; (8) + TAC. The line represents the least-squares linear fit of the data ($R = 0.9992$).

ACKNOWLEDGMENT

We are grateful to Olga Boudker for valuable discussions, and to Amnon Horovitz for the critical reading of the manuscript and valuable suggestions. We thank Talia Miron and Aharon Rabinkow for the gifts of [^{3}H]-allicin and allicin, respectively, Terry Rosenberry for recombinant human AChE, and Joel Sussman for help in the preparation of Figure 13.

REFERENCES

1. Privalov, P. L., and Gill, S. J. (1988) Stability of protein structure and hydrophobic interaction. *Adv. Protein Chem. 39*, 191–234.
2. Pace, C. N. (1990) Conformational stability of globular proteins. *Trends Biotech. 8*, 93–98.
3. Kern, S., Riester, D., Hildmann, C., Schwienhorst, A., and Meyer-Almes, F.-J. (2007) Inhibitor-mediated stabilization of the conformational structure of a histone deacetylase-like amidohydrolase. *FEBS J. 274*, 3578–3588.
4. Sawkar, A. R., Cheng, W. C., Beutler, E., Wong, C. H., Balch, W. E., and Kelly, J. W. (2002) Chemical chaperones increase the cellular activity of N370S beta-glucosidase: a therapeutic strategy for Gaucher disease. *Proc. Natl. Acad. Sci. U.S.A. 99*, 15428–15433.
5. Kuryatov, A., Luo, J., Cooper, J., and Lindstrom, J. (2005) Nicotine acts as a pharmacological chaperone to up-regulate human alpha4beta2 acetylcholine receptors. *Mol. Pharmacol. 68:* 1839–1851.
6. Yu, Z., Sawkar, A. R., and Kelly, J. W. (2007) Pharmacologic chaperoning as a strategy to treat Gaucher disease. *FEBS J. 274*, 4944–4950.
7. Fan, J. Q. (2008) A counterintuitive approach to treat enzyme deficiencies: use of enzyme inhibitors for restoring mutant enzyme activity. *Biol. Chem. 389*, 1–11.
8. Quinn, D. M. (1987) Acetylcholinesterase: enzyme structure, reaction dynamics, and virtual transition states. *Chem. Rev. 87*, 955–979.
9. Massoulié, J. (2002) The origin of the molecular diversity and functional anchoring of cholinesterases. *Neurosignals 11*, 130–143.
10. Sussman, J. L., Harel, M., Frolow, F., Oefner, C., Goldman, A., Toker, L., and Silman, I. (1991) Atomic structure of acetylcholinesterase from Torpedo californica: a prototypic acetylcholine-binding protein. *Science 253*, 872–879.
11. Morel, N., Bon, S., Greenblatt, H. M., Van Belle, D., Wodak, S. J., Sussman, J. L., Massoulié, J., and Silman, I. (1999) Effect of mutations within the peripheral anionic site on the stability of acetylcholinesterase. *Mol. Pharmacol. 55*, 982–992.
12. Taylor, P., and Radic, Z. (1994) The cholinesterases: from genes to proteins. *Annu. Rev. Pharmacol. Toxicol. 34*, 281–320.
13. Kaplan, D., Ordentlich, A., Barak, D., Ariel, N., Kronman, C., Velan, B., and Shafferman, A. (2001) Does "butyrylization" of acetylcholinesterase through substitution of the six divergent aromatic amino acids in the active center gorge generate an enzyme mimic of butyrylcholinesterase? *Biochemistry 40*, 7433–7445.
14. Greenblatt, H. M., Dvir, H., Silman, I., and Sussman, J. L. (2003) Acetylcholinesterase: a multifaceted target for structure-based drug design of anticholinesterase agents for the treatment of Alzheimer's disease. *J. Mol. Neurosci. 20*, 369–383.
15. Dolginova, E. A., Roth, E., Silman, I., and Weiner, L. M. (1992) Chemical modification of *Torpedo* acetylcholinesterase by disulfides: Appearance of a "molten globule" state. *Biochemistry 31*, 12248–12254.
16. Kreimer, D. I., Dolginova, E. A., Raves, M., Sussman, J. L., Silman, I., and Weiner, L. (1994) A metastable state of Torpedo californica acetylcholinesterase generated by modification with organomercurials. *Biochemistry 33*, 14407–14418.
17. Weiner, L., Kreimer, D., Roth, E., and Silman, I. (1994) Oxidative stress transforms acetylcholinesterase to a molten-globule-like state. *Biochem. Biophys. Res. Commun. 198*, 915–922.
18. Kreimer, D. I., Shnyrov, V. L., Villar, E., Silman, I., and Weiner, L. (1995) Irreversible thermal denaturation of Torpedo californica acetylcholinesterase. *Protein Sci. 4*, 2349–2357.
19. Kreimer, D. I., Szosenfogel, R., Goldfarb, D., Silman, I., and Weiner, L. (1994) Two-state transition between molten globule and unfolded states of acetylcholinesterase as monitored by electron paramagnetic resonance spectroscopy. *Proc. Natl. Acad. Sci. U.S.A. 91*, 12145–12149.
20. Millard, C. B., Shnyrov, V. L., Newstead, S., Shin, I., Roth, E., Silman, I., and Weiner, L. (2003) Stabilization of a metastable state of Torpedo californica acetylcholinesterase by chemical chaperones. *Protein Sci. 12*, 2337–2347.
21. Tatzelt, J., Prusiner, S. B., and Welch, W. J. (1996) Chemical chaperones interfere with the formation of scrapie prion protein. *EMBO J. 15*, 6363–6373.
22. Payne, C. S., Saeed, M., and Wolfe, A. D. (1989) Ligand stabilization of cholinesterases. *Biochim. Biophys. Acta 999*, 46–51.
23. Rochu, D., Clery-Barraud, C., Renault, F., Chevalier, A., Bon, C., and Masson, P. (2006) Capillary electrophoresis versus differential scanning calorimetry for the analysis of free enzyme versus enzyme-ligand complexes: in the search of the ligand-free status of cholinesterases. *Electrophoresis 27*, 442–451.
24. Khramtsov, V. V., Yelinova, V. I., Weiner, L. M., Berezina, T. A., Martin, V. V., and Volodarsky, L. B. (1989) Quantitative determination of SH groups in low- and high-molecular-weight compounds by an electron spin resonance method. *Anal. Biochem. 182*, 58–63.
25. Sussman, J. L., Harel, M., Frolow, F., Varon, L., Toker, L., Futerman, A. H., and Silman, I. (1988) Purification and crystallization of a dimeric form of acetylcholinesterase from *Torpedo californica* subsequent to solubilization with phosphatidylinositol-specific phospholipase C. *J. Mol. Biol. 205*, 821–823.
26. Ralston, J. C., Rush, R. S., Doctor, B. P., and Wolfe, D. (1985) Acetylcholinesterase from fetal bovine serum. Purification and characterization of soluble G_4 enzyme. *J. Biol. Chem. 260*, 4312–4318.
27. Mallender, W. L., Szegletes, T., and Rosenberry, T. L. (1999) Organophosphorylation of acetylcholinesterase in the presence of peripheral site ligands. Distinct effects of propidium and fasciculin. *J. Biol. Chem. 274*, 8491–8499.
28. Eastman, J., Wilson, E. J., Cerveñansky, C., and Rosenberry, T. L. (1995) Fasciculin 2 binds to the peripheral site on acetylcholinesterase and inhibits substrate hydrolysis by slowing a step involving proton transfer during enzyme acylation. *J. Biol. Chem. 270*, 19694–19701.
29. Ellman, G. L., Courtney, K. D., Andres, V, and Featherstone, R. M. A new and rapid colorimetric determination of acetylcholinesterase activity. *Biochem. Pharmacol. 7*, 88–95.
30. Berman, H. A., and Leonard, K. (1992) . Interaction of tetrahydroaminoacridine with acetylcholinesterase and butyrylcholinesterase. *Mol. Pharmacol. 41*, 412–418.
31. Lopez Mayorga, O., and Freire, E. (1987) Dynamic analysis of differential scanning calorimetry data. *Biophys. Chem. 87*, 87–96.
32. Lumry, R., and Eyring, H. (1954) . Conformation changes of proteins. *J. Phys. Chem. 58*, 110–120.
33. Kurganov, B. I., Lyubarev, A. E., Sanchez-Ruiz, J. M., and Shnyrov, V. L. (1997) Analysis of differential scanning calorimetry data for proteins. Criteria of validity of one-step mechanism of irreversible protein denaturation. *Biophys. Chem. 69*, 125–135.
34. Austin, L., and Berry, W. K. (1953) Two selective inhibitors of cholinesterase. *Biochem. J. 54*, 695–700.
35. Heilbronn, E. (1961) Inhibition of cholinesterases by tetrahydroaminoacridine. *Acta Chem. Scand. 15*, 1386–1390.
36. Radic, Z., Duran, R., Vellom, D. C., Li, Y., Cerveñansky, C., and Taylor, P. (1994) Site of fasciculin interaction with acetylcholinesterase. *J. Biol. Chem. 269*, 11233–11239.
37. Harel, M., Kleywegt, G. J., Ravelli, R. B., Silman, I., and Sussman, J. L. (1995) Crystal structure of an acetylcholinesterase-fasciculin complex: interaction of a three-fingered toxin from snake venom with its target. *Structure 3*, 1355–1366.
38. Bourne, Y., Taylor, P., Radic, Z., and Marchot, P. (2003) . Structural insights into ligand interactions at the acetylcholinesterase peripheral anionic site. *EMBO J. 22*, 1–12.
39. Golicnik, M., and Stojan, J. (2002) Multi-step analysis as a tool for kinetic parameter estimation and mechanism discrimination in the reaction between tight-binding fasciculin 2 and electric eel acetylcholinesterase. *Biochim. Biophys. Acta 1597*, 164–172.
40. Cousin, X., Bon, S., Duval, N., Massoulié, J., and Bon, C. (1996) Cloning and expression of acetylcholinesterase from Bungarus fasciatus venom. A new type of cooh-terminal domain; involvement of a positively charged residue in the peripheral site. *J. Biol. Chem. 271*, 15099–15108.
41. Steinberg, N., Roth, E., and Silman, I. (1990) Torpedo acetylcholinesterase is inactivated by thiol reagents. *Biochem. Int. 21*, 1043–1050.
42. Weiner, L. M. (1995) Quantitative determination of thiol groups in low and high molecular weight compounds by electron paramagnetic resonance. *Methods Enzymol. 251*, 87–105.
43. Weiner, L. M. (2007) Stable nitroxyl radicals as pH, thiol and electron transfer probes. *Appl. Magn. Reson. 31*, 357–373.
44. Miron, T., Bercovici, T., Rabinkov, A., Wilchek, M., and Mirelman, D. (2004) [3 H]-Allicin: preparation and applications. *Anal. Biochem. 15*, 364–369.

45. Harel, M., Schalk, I., Ehret-Sabatier, L., Bouet, F., Goeldner, M., Hirth, C., Axelsen, P. H., Silman, I., and Sussman, J. L. (1993) Quaternary ligand binding to aromatic residues in the active-site gorge of acetylcholinesterase. *Proc. Natl. Acad. Sci. U.S.A. 90*, 9031–90355.
46. Sanchez-Ruiz, J. M. (1992) Theoretical analysis of Lumry-Eyring models in differential scanning calorimetry. *Biophys. J. 61*, 921–935.
47. Clark, D. Y., and Higgins, K. A. (1992) NMR Studies of Ligand-Macromolecular Interactions, in *Annual Reports on NMR Spectroscopy* (Webb, G. A., Ed.) Vol. 22, pp 61−138, Academic Press, New York.
48. Li, Y., Li, Q., Sun, M., Song, G., Jiang, S., and Zhu, D. (2004) 1 H NMR relaxation investigation of acetylcholinesterase inhibitors from huperzine A and derivative. *Bioorg. Med. Chem. Lett. 14*, 1585–1588.
49. Delfini, M., Di Cocco, M. E., Piccioni, F., Porcelli, F., Borioni, A., Rodomonte, A., and Del Giudice, M. R. (2007) Tacrine derivatives-acetylcholinesterase interaction: 1 H NMR relaxation study. *Bioorg. Chem. 35*, 243–257.
50. Holdgate, J. A., and Ward, W. H. J. (2005) Measurements of binding thermodynamics in drug discovery. *Drug Discovery Today 10*, 1543–1550.
51. Kryger, G., Harel, M., Giles, K., Toker, L., Velan, B., Lazar, A., Kronman, C., Barak, D., Ariel, N., Shafferman, A., Silman, I., and Sussman, J. L. (2000) Structures of recombinant native and E202Q mutant human acetylcholinesterase complexed with the snake-venom toxin fasciculin-II. *Acta Crystallogr., Sect. D 56*, 1385–1394.
52. Privalov, P. L. (1989) Thermodynamic problems of protein structure. *Annu. Rev. Biophys. Biophys. Chem. 18*, 47–69.
53. Eichler, J., Anselmet, A., Sussman, J. L., Massoulié, J., and Silman, I. (1994) Differential effects of "peripheral" site ligands on Torpedo and chicken acetylcholinesterase. *Mol. Pharmacol. 45*, 335–340.

BI801196Y